MAPAN-JOURNAL ,
Publisher: METROLOGY SOC INDIA ,
NPL PREMISES,
Address: DR K S KRISHNAN MARG,
NEW DELHI, INDIA, 110 012
ISSN / eISSN:0970-3950 / 0974-9853
Volume 26-Issue 1-(2026)
DOI:https://doi-001.org/1025/17773574897085

Research on Suppressing Electromechanical Oscillation Strategies in Dual-Machine Grid-Connected Systems Based on Additional Damping Control

Lihui Tian1a*

1.College of Electrical Engineering, Shanghai University of Electric Power, Shanghai 200090,Shanghai,China;.

Email: shunlishedu@163.com

Abstract: While renewable energy units bring low-carbon benefits, they also pose new challenges for power system regulation. Their characteristics of randomness, intermittency, and volatility exacerbate grid stability issues. Renewable energy units controlled by Virtual Synchronous Generator (VSG) technology can provide a certain level of inertia and damping support to the system. However, they also inherit the electromechanical characteristics of traditional Synchronous Generators (SGs) and may participate in dynamic interactions with synchronous units/control systems, potentially intensifying the risk of SG-like electromechanical oscillations in power systems. Addressing this issue, this paper investigates the mechanism of VSG-based power system SG-like electromechanical oscillations, analyzing the oscillation mechanisms in both single-VSG grid-connected systems and VSG-SG dual-machine grid-connected systems. Furthermore, to suppress these SG-like electromechanical oscillations in VSG-based power systems, an additional damping control-based suppression strategy is proposed. The general structure of the additional damping control is designed using a "lead-lag" phase compensation link. Phillips-Heffron models are constructed for both single-VSG and VSG-SG dual-machine grid-connected systems incorporating additional damping control. Using the Damping Torque Analysis (DTA) method, the pathways for SG-like electromechanical oscillation effects under additional damping control are analyzed. It is shown that the VSG virtual excitation regulator, when accounting for the additional damping control, provides positive damping torque to the VSG's SG-like electromechanical oscillation loop, thereby suppressing these oscillations in VSG-based power systems and enhancing system stability.

Keywords: Virtual Synchronous Generator (VSG); Additional Damping Control; SG-like Electromechanical Oscillation; Dual-Machine Grid-Connected System

1. Introduction

VSG emulates the governor system of an SG to provide virtual inertia to the system. When its capacity is comparable to slow-timescale control units and the system damping is weak, power disturbances can easily lead to overshoot and interactions due to non-synchronous responses [1], potentially triggering SG-like electromechanical oscillations [2]. Owing to its ability to mimic the electromechanical transient response characteristics of SGs, VSG technology has become a typical solution in the field of renewable energy grid integration control. The dynamic interactions of VSG during transients may exacerbate the original oscillation modes of SGs, leading to electromechanical oscillation modes dominated by VSG-SG dynamic interactions, posing a significant threat to the dynamic stability of modern power systems [3]. This type of electromechanical dynamic interaction arising from VSG-SG dual-machine grid-connected systems falls within the category of power-electronics-driven slow dynamic stability problems, with oscillation frequencies extending beyond the traditional electromechanical mode range of 0.1-2.5 Hz. This paper investigates suppression strategies for SG-like electromechanical oscillations based on their triggering mechanisms and key influencing factors within VSG-dominated systems, aiming to establish a comprehensive and multi-dimensional theoretical and methodological framework. This research provides theoretical support and guidance for ensuring the dynamic security and stability of new power systems under complex operating conditions.

2 Analysis of the Mechanism of Electromechanical Oscillation in Power Systems Based on VSG

2.1 Analysis of Electromechanical Oscillation Mechanism in VSG Single-Machine Grid-Connected System Type

Based on the established linearized model of the VSG single-machine grid-connected system, the VSG-type electromechanical oscillation modes are quantitatively analyzed, and the damping torque analysis method is adopted to reveal the mechanism of the VSG single-machine grid-connected system type electromechanical oscillation. Combining Equations (2.1) and (2.2), the Phillips-Heffron model of the VSG single-machine grid-connected system is constructed, as shown in Figure 1.

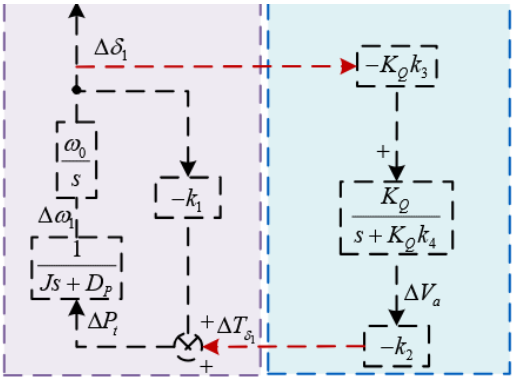

Figure 1 Phillips Heffron model of VSG single-machine grid-connected system

From the Phillips Heffron model of the VSG grid-connected system, it can be known that the damping torque input to the VSG-type electromechanical oscillation circuit is generated by its own virtual excitation regulator link, and the output power Angle of the VSG-type electromechanical oscillation circuit further affects its virtual excitation regulator link, forming a "closed-loop disturbance". Furthermore, based on the VSG single-machine grid-connected electromechanical oscillation circuit, Equation (2.1) can be obtained.

$$\Delta\ddot{\delta}_1 + \frac{D_P}{J}\Delta\dot{\delta}_1 + \frac{\omega_0 k_1}{J}\Delta\delta_1 + \frac{\omega_0 k_2 \Delta V_a}{J} = 0 \tag{2.1}$$

Equation (2.1) shows that the transfer function of the VSG virtual quasi-electromechanical oscillation loop directly determines the characteristics of the quasi-electromechanical oscillation mode. According to Figure 2.4, when $\Delta T_A = -k_A \Delta V_a$ acts on the VSG quasi-electromechanical oscillation loop, its magnitude is constrained by $\Delta\delta_1$. Under power disturbance, the change in the virtual power angle is fed back to the VSG quasi-electromechanical oscillation loop through the phase lag characteristic of the virtual excitation regulator, thereby affecting the stability of the VSG itself, which is detrimental to the stable operation of the VSG single-machine grid-connected system. To further explore the mechanism of quasi-electromechanical oscillation in the VSG single-machine grid-connected system, based on the traditional DTA, the input signal ΔT_A is decomposed into Equation (2.2).

$$\Delta T_A = T_\omega \Delta\omega_1 + T_\delta \Delta\delta_1 \tag{2.2}$$

where $T_\omega \Delta\omega_1$ is the damping torque provided by the VSG virtual excitation regulator to the VSG quasi-electromechanical oscillation loop, and $T_\delta \Delta\delta_1$ is the synchronous torque provided by the VSG virtual excitation regulator to the VSG quasi-electromechanical oscillation loop.

Combining Equations (2.1) and (2.2) yields Equation (2.3).

$$\Delta\ddot{\delta}_1 + \frac{D_P}{J} + T_\omega \Delta\dot{\delta}_1 + \frac{\omega_0 k_1}{J}\Delta\delta_1 += 0 \tag{2.3}$$

According to Equation (2.3), the amplitude characteristics of the damping torque T_ω determine the damping characteristics of the quasi-electromechanical oscillation mode in the VSG single-machine grid-connected system. When the damping torque T_ω provided by the VSG virtual excitation regulator to the VSG quasi-electromechanical oscillation loop falls below a critical threshold or exhibits negative damping characteristics, it will further exacerbate the risk of quasi-electromechanical oscillation in the system. Appropriately increasing the damping torque T_ω to provide positive damping torque for the system can enhance system stability.

2.2.2 Analysis of Factors Influencing Quasi-Electromechanical Oscillation in VSG Single-Machine Grid-Connected System

In VSG control, the damping coefficient *Dp* is the core dynamic parameter for suppressing quasi-electromechanical oscillations, directly determining the system's transient energy dissipation capability. The moment of inertia *J*, as the key control variable for inertial support strength, governs the system's dynamic response to frequency disturbances. Therefore, the coordinated optimization of these two is fundamental to ensuring stable operation of the VSG single-machine grid-connected system. This section further reveals the dynamic response characteristics of quasi-electromechanical oscillation in the VSG single-machine grid-connected system under variations of moment of inertia *J* and damping coefficient *Dp*.

The VSG single-machine grid-connected system is built in Simulink, with its relevant parameters shown in Table 1. A power disturbance is set at t=1s, and different damping coefficients *Dp* and moments of inertia *J* are configured. When the moment of inertia *J*=6 and *Dp* varies, the active power and virtual power angle of the VSG are shown in Figure 2. When the damping coefficient *Dp* =20 and *J* varies, the active power and virtual power angle of the VSG are shown in Figure 2.

Table 2.1 Related Parameters of VSG Single-Machine Grid-Connected System

System Parameter	Value (p.u.)	System Parameter	Value (p.u.)	System Parameter	Value (p.u.)
P_{ref}	0.5	Q_{ref}	0.1	X_{ag}	0.3
K_Q	1	V_{ref}	1	V_g	1

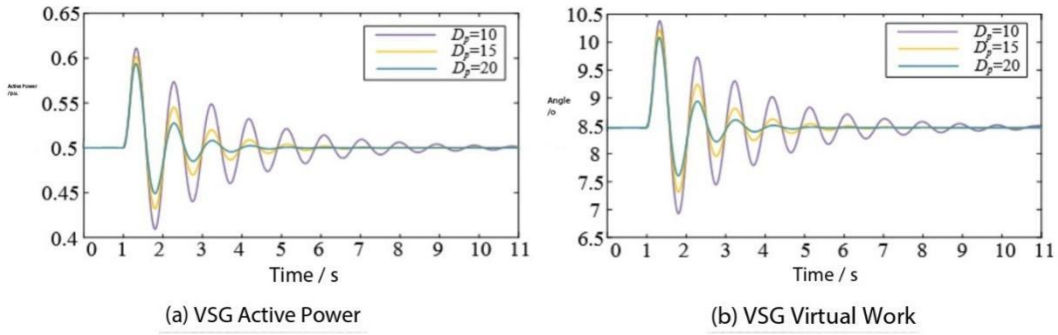

Figure 2 Active Power Response and Virtual Power Angle of VSG when J=6, Dp varies

(a) VSG Active Power (b) VSG Virtual Power Angle

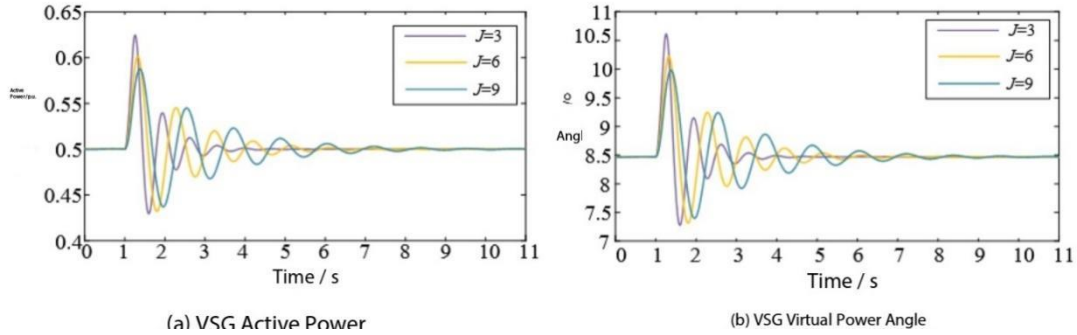

Figure 3 Active Power Response and Virtual Power Angle of VSG when Dp=20, J varies

(a) VSG Active Power (b) VSG Virtual Power Angle

The analysis of simulation results indicates that the damping coefficient *Dp*, as a key parameter for transient energy dissipation, significantly affects only the amplitude of the VSG active power dynamic response and virtual power angle fluctuations, while the system oscillation frequency remains relatively constant. A smaller *Dp* value leads to larger oscillation amplitudes in the VSG active power output and virtual power angle, exerting a greater influence on the quasi-electromechanical oscillation of the VSG single-machine grid-connected system and weakening the system's oscillation damping characteristics. The moment of inertia *J*, as the core variable for inertial support strength, affects both the oscillation amplitude and frequency of the VSG active power output and virtual power angle. After a system disturbance, a smaller *J* results in higher oscillation amplitudes for the VSG active power and virtual power angle, but the system oscillation recovers quickly to stability when *J* is small. Therefore, the coordinated optimization of *Dp* and *J* can effectively balance the system's dynamic response and reduce the risk of quasi-

electromechanical oscillation in the VSG single-machine grid-connected system.

3. Electromechanical oscillation suppression strategy based on additional damping control

3.1 Design of Auxiliary Damping Control Structure

The auxiliary damping control proposed in this paper uses a "lead-lag" phase compensation link as its fundamental structure. It takes the VSG angular frequency deviation and the active power deviation as inputs, and outputs the reactive power deviation, forming a control architecture with bidirectional regulation capability. Its mathematical model is shown in Figure 4.

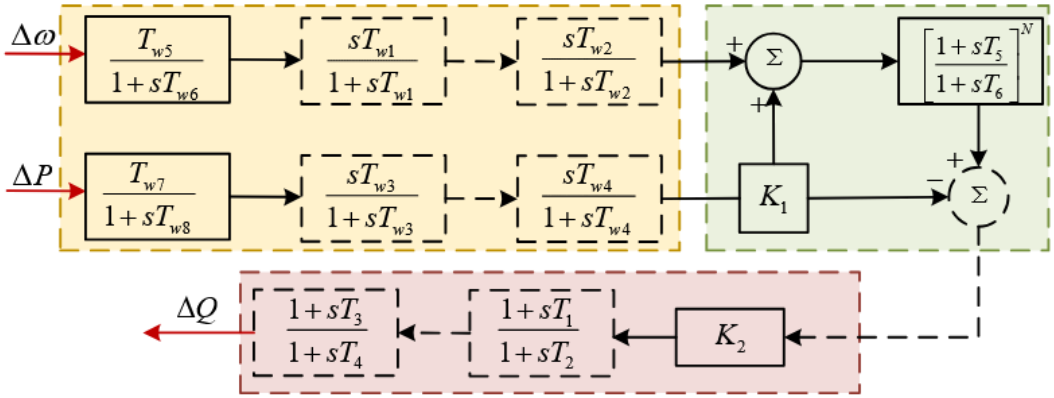

Figure 4 Mathematical model of auxiliary damping control

In Figure 4, Δω is the deviation of the VSG's virtual angular frequency, ΔP is the deviation of the VSG's output active power, Tw1–Tw8 are the time constants of the washout (high-pass) filters (set as Tw1 = Tw2 = Tw3 = Tw4 = 6, Tw6 = Tw8 = 0.02, Tw5 = Tw7 = 0.46), K1 is the gain coefficient of the power deviation amplification link, T5 and T6 are the time constants of the filter links (set as T5 = 0.2, T6 = 0.1, N = 5), K2 is the gain coefficient of the auxiliary damping control amplification link, and T1–T4 are the time constants of the auxiliary damping control phase compensation links.

The VSG's virtual angular frequency deviation Δω and output active power deviation ΔP serve as the input signals, and the reactive power deviation ΔQ serves as the output signal. Let the transfer function of the auxiliary damping control "lead-lag" link be F_ADC(s), then:

$$G_c(s) = K \cdot \frac{1+sT_1}{1+sT_2} \tag{3.1}$$

where K2 is the gain coefficient of the auxiliary damping control amplification link, and T1–T4 are the time constants of the auxiliary damping control phase compensation links.

Let the signals after the washout filters be Δω' and ΔP' respectively. The complete transfer function of the auxiliary damping control structure can then be expressed as:

$$\Delta Q = ((\Delta\omega' + K_1\Delta P')[\frac{1+sT_5}{1+sT_6}]^N - K_1\Delta P)F_{\mathrm{ADC}}(s) \tag{3.2}$$

$$\Delta\omega' = \Delta\omega \times \frac{T_{w5}}{1+sT_{w6}} \times \frac{sT_{w1}}{1+sT_{w1}} \times \frac{sT_{w2}}{1+sT_{w2}} \tag{3.3}$$

$$\Delta P' = \Delta P \times \frac{T_{w7}}{1+sT_{w8}} \times \frac{sT_{w3}}{1+sT_{w3}} \times \frac{sT_{w4}}{1+sT_{w4}} \tag{3.4}$$

Introducing variables A and B:

$$A = \Delta\omega \times \frac{T_{w5}}{1+sT_{w6}} \times \frac{sT_{w1}}{1+sT_{w1}} \times \frac{sT_{w2}}{1+sT_{w2}} \times [\frac{1+sT_5}{1+sT_6}]^N$$

$$B = K_1\Delta P \times \frac{T_{w7}}{1+sT_{w8}} \times \frac{sT_{w3}}{1+sT_{w3}} \times \frac{sT_{w4}}{1+sT_{w4}} \times [\frac{1+sT_5}{1+sT_6}]^N \tag{3.5}$$

Thus, the transfer function of the auxiliary damping control structure can be expressed as:

$$\Delta Q = (A + B - K_1\Delta P)F_{\mathrm{ADC}}(s) \tag{3.6}$$

where ΔQ is the output reactive power deviation of the auxiliary damping control, and F_ADC(s) corresponds to the transfer function of the auxiliary damping control added to the reactive power loop of the VSG virtual excitation system.

Let the overall auxiliary damping control transfer function be H_ADC(s), then:

$$H_{\mathrm{ADC}}(S) = (\mathrm{A} + B - K_1\Delta P)F_{\mathrm{ADC}}(S) \tag{3.7}$$

3.2 Case Study Analysis

3.2.1 Suppression of Quasi-Electromechanical Oscillations in VSG Single-Machine Grid-Connected System Based on Auxiliary Damping Control

To verify the theoretical feasibility of parameter setting for auxiliary damping control based on DTA, a VSG single-machine grid-connected system (Figure 1) was built in MATLAB/Simulink. Four different operating conditions were set for the VSG single-machine grid-connected system, as shown in Table 3.1. Condition I represents the classic normal operation state of the system; Condition II represents the system operation state with a higher VSG penetration rate; considering the flexible adjustable parameters of VSG, Condition III represents the system operation state with reasonably set VSG control parameters; Condition IV represents the system operation state with unreasonably set VSG control parameters, aiming to test the adaptability of the auxiliary damping control.

Table 3.1 Parameters of VSG Single-Machine Grid-Connected System Under Different Operating Conditions

System Parameter (p.u.)	Condition I	Condition II	Condition III	Condition IV
Pref	0.5	0.6	0.5	0.5
Qref	0.1	0.1	0.1	0.1
Dp	20	20	15	20
J	5	6	3	15
KQ	1	1	1	1
Vref	1	1	1	1
Xag	0.3	0.3	0.3	0.3
Vg	1	1	1	1

Four sets of typical operating scenarios were used for comparative verification. By substituting the system parameters of each condition into Equation (2.3), the characteristics of the quasi-electromechanical oscillation modes of the VSG single-machine grid-connected system without auxiliary damping control were obtained by solving. To further evaluate the time-varying adaptability of the auxiliary damping control strategy, Tables 3.2 and 3.3 respectively show the quasi-electromechanical oscillation modes before and after introducing auxiliary damping control at two different operating points: t=0.8s and t=2s. The relevant parameters of the auxiliary damping control are shown in Table 3.4.

Table 3.2 Quasi-electromechanical oscillation modes of VSG single-machine grid-connected system before and after auxiliary damping control integration (t=0.8s)

Condition	**Before Auxiliary Damping Control Integration**		**After Auxiliary Damping Control Integration**	
	Eigenvalue	Damping Ratio	Eigenvalue	Damping Ratio
Condition I	-2.04 ± j11.4	0.14	-6.36 ± j15.8	0.375
Condition II	-1.72 ± j13.1	0.13	-6.76 ± j13.3	0.461
Condition III	-2.54 ± j18.6	0.135	-5.54 ± j20.6	0.26
Condition IV	-0.7 ± j8.35	0.0835	-6.91 ± j8.59	0.627

Table 3.3 Quasi-electromechanical oscillation modes of VSG single-machine grid-connected

system before and after auxiliary damping control integration (t=2s)

Condition	Before Auxiliary Damping Control Integration		After Auxiliary Damping Control Integration	
	Eigenvalue	Damping Ratio	Eigenvalue	Damping Ratio
Condition I	-2.04 ± j14.4	0.14	-5.99 ± j14.7	0.379
Condition II	-1.74 ± j13	0.132	-7.07 ± j13.9	0.454
Condition III	-2.53 ± j18.58	0.135	-5.53 ± j20.6	0.259
Condition IV	-0.706 ± j8.34	0.0843	-6.89 ± j8.67	0.622

Table 3.4 Values of auxiliary damping control parameters for VSG single-machine grid-connected system under different operating conditions

Auxiliary Damping Control Parameter	Condition I	Condition II	Condition III	Condition IV
T1	0.318	0.31	0.279	0.138
T2	0.002	0.002	0.002	0.002
T3	0.318	0.31	0.279	0.138
T4	0.002	0.002	0.002	0.002
K2	-0.2	-0.3	-0.575	-1.784

Based on the auxiliary damping control related parameters in Table 3.4, the eigenvalues of the system after integrating the auxiliary damping control were calculated and compared with the conditions without auxiliary damping control. The trajectories of the quasi-electromechanical oscillation mode changes of the system at t=0.8s and t=2s under the four conditions are obtained, as shown in Figures 5-8. From the zero-pole plots, it can be clearly seen that under the four operating conditions set in Tables 3.3 and 3.4, for the two different operating points (t=0.8s and t=2s), the pole position moves from λ1 to λ2 before and after adding the auxiliary damping control to the system.

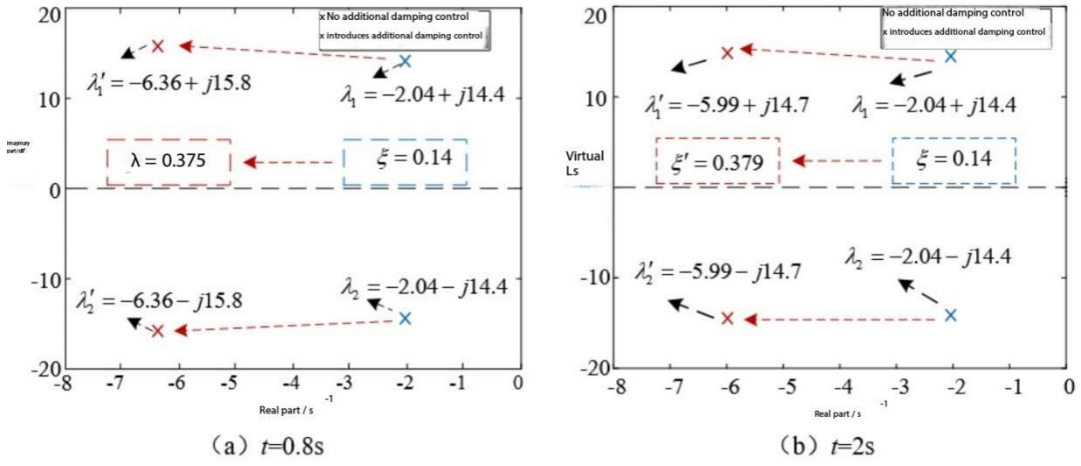

Figure 5 Condition I: Zero-pole plots of VSG single-machine grid-connected system before and

after auxiliary damping control integration

According to Figure 5, linearized analysis was performed on the VSG single-machine grid-connected system at t=0.8s and t=2s, respectively. Under Condition I, where the system is in the classic normal operation state, the system damping ratio before introducing auxiliary damping control was 0.14. After introducing auxiliary damping control, the system damping ratio after linearization at both t=0.8s and t=2s increased. The system damping ratio corresponding to t=0.8s was 0.375, and that corresponding to t=2s was 0.379, representing increases of approximately 167.86% and 170.71%, respectively. The analysis results show that the proposed auxiliary damping control strategy effectively enhances the system's dynamic damping characteristics, which is beneficial for suppressing the amplitude response of quasi-electromechanical oscillations.

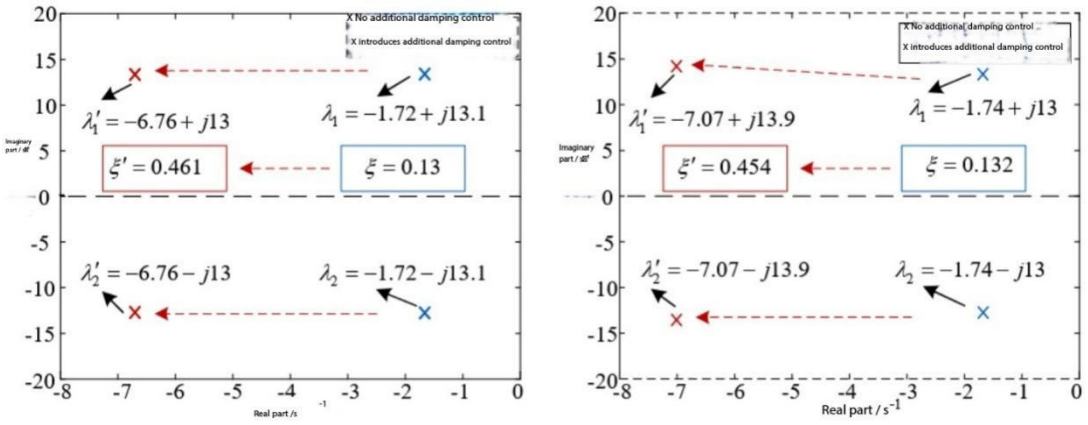

（a）t=0.8s　　（b）t=2s

Figure 6 Condition II: Zero-pole plots of VSG single-machine grid-connected system before and after auxiliary damping control integration

According to Figure 6, before and after adding auxiliary damping control to the system, the pole position moves left from λ1 to λ2', and the system damping ratio increases significantly. Linearized analysis was performed on the VSG single-machine grid-connected system at t=0.8s and t=2s, respectively. Under Condition II, which is the system operating state with a higher VSG penetration rate, before introducing auxiliary damping control, the system damping ratio corresponding to t=0.8s was 0.13, and that corresponding to t=2s was 0.132. After introducing auxiliary damping control, the damping ratios increased, with values of 0.461 and 0.454 for t=0.8s and t=2s, respectively, representing increases of approximately 254.6% and 243.9%. The analysis shows that even under high VSG penetration rates, quasi-electromechanical oscillations in the VSG single-

machine grid-connected system based on auxiliary damping control are significantly weakened.

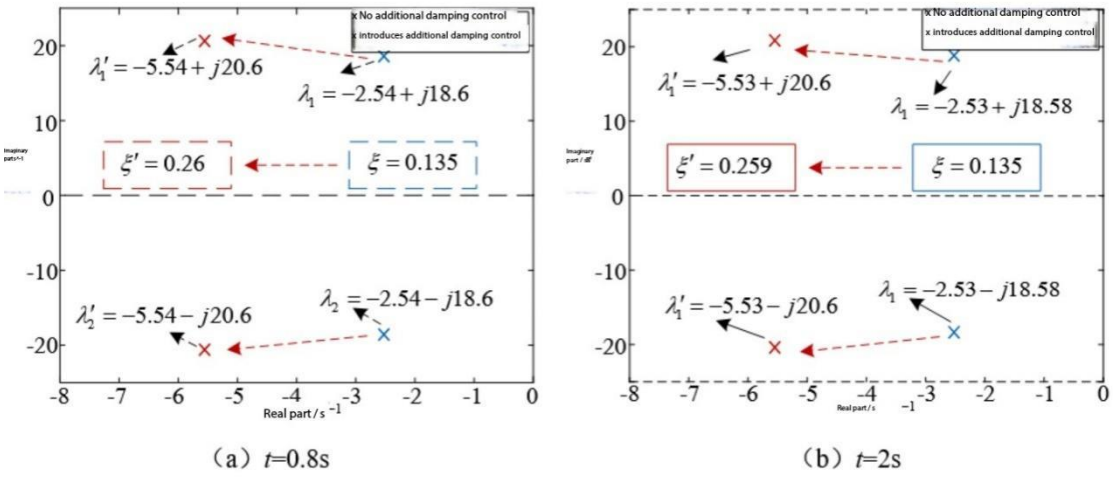

Figure 7 Condition III: Zero-pole plots of VSG single-machine grid-connected system before and after auxiliary damping control integration

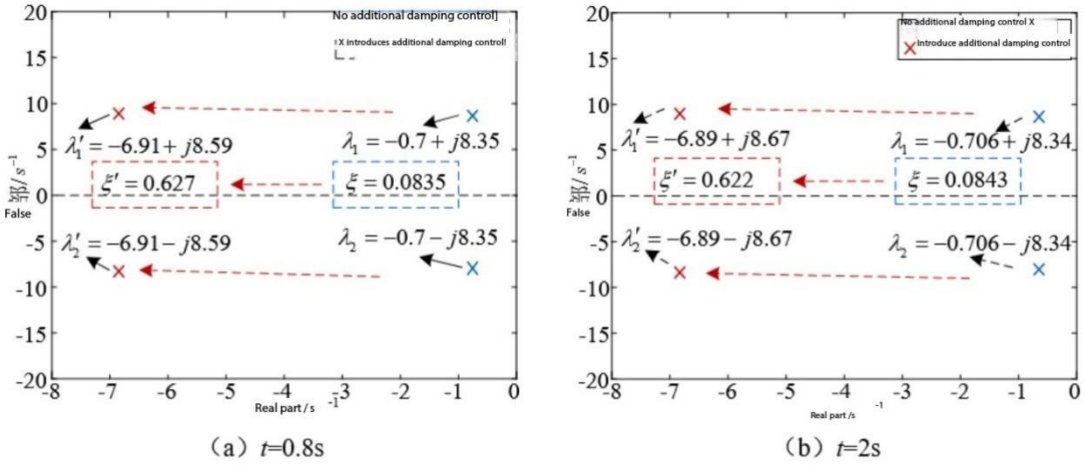

Figure 8 Condition IV: Zero-pole plots of VSG single-machine grid-connected system before and after auxiliary damping control integration

From the simulation results in Figures 7 and 8, it can be seen that for Condition IV, even though the VSG control parameters are unsuitable, after adding auxiliary damping control, the damping change of the quasi-electromechanical oscillation mode is significant. At both t=0.8s and t=2s, it changes from a low damping state to a high damping state. Compared with Condition III, the damping change is more pronounced, which indicates that the setting of VSG control parameters has a greater impact on the auxiliary damping control.

The above multi-condition simulation analysis shows that under different operating conditions, the quasi-electromechanical oscillation characteristics of the system vary. Root locus analysis shows

that the introduction of auxiliary damping control causes the eigenvalues of the dominant mode to shift to the left, further indicating that auxiliary damping control improves system stability to a certain extent, verifying the applicability of the DTA-based parameter tuning strategy at time-varying operating points.

To further verify the robustness of the proposed oscillation suppression strategy, a VSG grid-connected system based on auxiliary damping controller was built in MATLAB/Simulink. The parameters of the auxiliary damping control are determined based on the detailed calculation results in Table 3.5. The system parameters for the four typical operating scenarios are shown in Table 3.1. A power disturbance is set at the grid connection point g at t=1s. Based on whether the auxiliary damping control is introduced into the VSG single-machine grid-connected system, the VSG active power output and virtual power angle before and after introducing auxiliary damping control under the four conditions are shown in Figures.

According to the analysis of dynamic response characteristics in Figure 9, under Condition I, the VSG grid-connected system exhibits static stable operation characteristics before disturbance, with VSG active power output maintained at 0.5 p.u. and virtual power angle at approximately 8.49°. After a power disturbance occurs in the system, both the VSG active power output and its virtual power angle oscillate. The system recovers from transient oscillation to steady-state operation in about 6.5 seconds. After introducing auxiliary damping control, the system's dynamic performance improves significantly. The system converges to the original steady-state value within 3.5 seconds. The virtual power angle after returning to the stable operating point is approximately 8.49°, and the active power output is 0.5 p.u., consistent with the static stable values before the system was disturbed. Analysis shows that auxiliary damping control reduces the system's transient recovery time by approximately 46.15%, which is significantly shorter than the time to recover stability under conditions without auxiliary damping control.

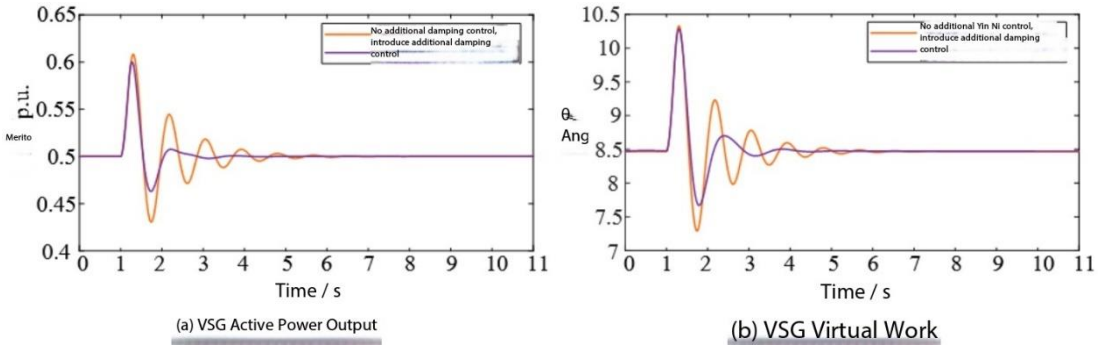

Figure 9 Condition I: VSG active power output and virtual power angle before and after auxiliary damping control integration

For Condition II, when the system is in the operating condition with a high VSG penetration rate, both the VSG active power output and its virtual power angle oscillate due to power disturbance. According to the simulation results in Figure 3.11, both the VSG active power output and its virtual power angle can maintain static stability before the system is disturbed. At this time, the VSG active power output is maintained at 0.6 p.u., and the virtual power angle is about 10.25°. The system recovers from transient oscillation to steady-state operation in about 7.3 seconds. After introducing auxiliary damping control, the system converges to the original steady-state value within 4.6 seconds. The active power converges to 0.7 p.u., and the virtual power angle converges to approximately 12.03°. However, the time for the system to return to stable operation after adding auxiliary damping control is significantly shortened, indicating that the damping characteristics of the VSG single-machine grid-connected system based on auxiliary damping control are significantly improved.

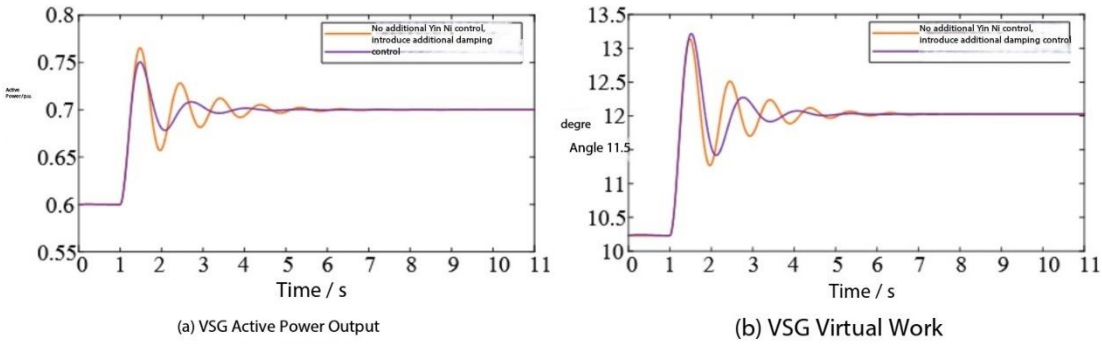

Figure 10 Condition II: VSG active power output and virtual power angle before and after auxiliary damping control integration

According to the VSG dynamic response characteristics shown in Figure 11, under Condition III,

the VSG initially operates stably at the active power reference value of 0.5 p.u., and its virtual power angle converges to the static equilibrium point of 8.49°. After a power disturbance occurs in the system, the VSG active power and virtual power angle exhibit decaying oscillation characteristics. The system recovers to steady-state operation after 6.7 seconds. After introducing auxiliary damping control, the system's dynamic convergence rate increases significantly. The VSG active power output and virtual power angle return to the original steady-state equilibrium point within 2.8 seconds, reducing the transient recovery time by approximately 58.21%. The analysis shows that auxiliary damping control effectively suppresses the quasi-electromechanical oscillations of the VSG single-machine grid-connected system by dynamically adjusting the damping torque component.

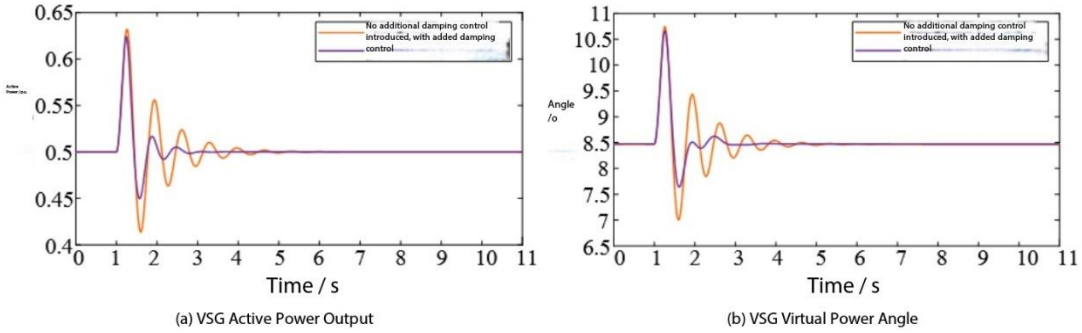

(a) VSG Active Power Output (b) VSG Virtual Power Angle

Figure 11 Condition III: VSG active power output and virtual power angle before and after auxiliary damping control integration

Comparing the simulation results in Figures 11 and 12, when the system parameters are set unreasonably, the system requires a longer time to recover to the pre-disturbance stable state after a power disturbance compared to Condition III. For Condition IV, when the VSG control parameters are set unreasonably, the system is in an oscillatory unstable state. After introducing auxiliary damping control, the system's dynamic response characteristics improve significantly, and the oscillation convergence after disturbance accelerates noticeably. However, compared to Condition III, it still takes a certain amount of time to recover to a stable state, indicating that system damping is improved after adding auxiliary damping control.

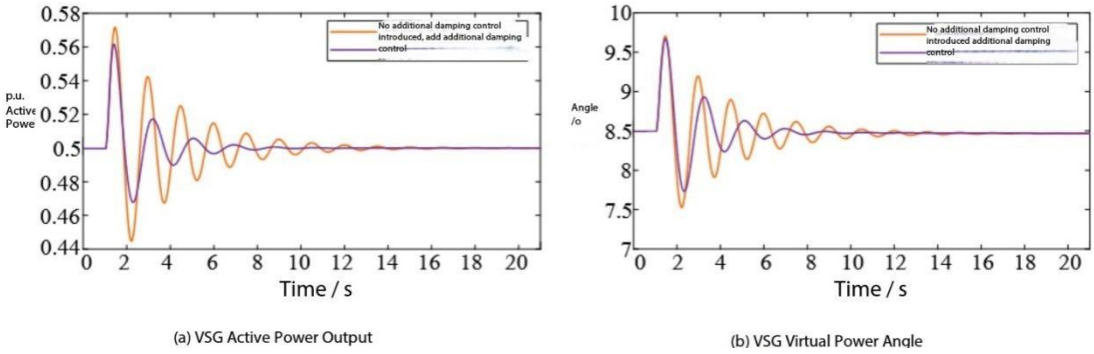

Figure 12 Condition IV: VSG active power output and virtual power angle before and after auxiliary damping control integration

In summary, comparative analysis shows that after adding auxiliary damping control, the system oscillation frequency increases slightly under all four conditions, and the system damping characteristics improve significantly, which is beneficial for suppressing quasi-electromechanical oscillations in the VSG single-machine grid-connected system.

3.2.2 Suppression of Quasi-Electromechanical Oscillations in VSG-SG Dual-Machine Grid-Connected System Based on Auxiliary Damping Control

To verify the effectiveness of auxiliary damping control in suppressing quasi-electromechanical oscillations in the VSG-SG dual-machine grid-connected system and the theoretical feasibility of parameter setting for auxiliary damping control based on DTA, a VSG-SG dual-machine grid-connected system (Figure 6) was built in MATLAB/Simulink. Based on the influence patterns of key control variables on the root locus of the dominant mode in the VSG-SG system from Chapter 2, four sets of typical boundary conditions were selected as test conditions, as shown in Table 3.5. Other system parameters are listed in Table 2.2. Among them, Condition I represents the operating state where SG power output and VSG penetration rate simultaneously approach the critical threshold (Pm = 0.7, Pref = 0.5); Condition II represents the operating state where SG operates overloaded with low VSG penetration rate (Pm = 0.8, Pref = 0.4); Condition III represents the system operation mode with low SG power output and high VSG penetration rate (Pm = 0.5, Pref = 0.7); Condition IV observes the impact of the VSG filter branch equivalent reactance exceeding the limit (Xac = 0.5) on system dynamic characteristics.

Table 3.5 System Parameters Under Different Operating Conditions of VSG-SG Dual-Machine Grid-Connected System

System Parameter (p.u.)	Condition I	Condition II	Condition III	Condition IV
Dp	1.2	0.9	2.23	1.17
J	0.01	0.0087	0.0562	0.0103
Pm	0.7	0.8	0.5	0.7
Pref	0.5	0.4	0.7	0.5
Xac	0.3	0.3	0.3	0.5

The quasi-electromechanical oscillation modes of the system under the four typical test conditions can be obtained from Equation. Combined with DTA principle analysis, it shows that the auxiliary damping control strategy can achieve a leftward shift of the eigenvalues of the dominant oscillation mode by directionally adjusting the damping torque component while maintaining the integrity of the synchronous torque. The quasi-electromechanical oscillation modes after introducing auxiliary damping control are shown in Table 3.6. The main key parameters of the auxiliary damping control are solved and shown in Table 3.7. Based on the DTA-tuned auxiliary damping control parameters shown in Table 3.7, the eigenvalues of the system after integrating the auxiliary damping control are calculated and compared with the conditions without auxiliary damping control. The evolution of the root locus of the system's dominant oscillation modes under the four typical test conditions is obtained, as shown in Figure 13.

Table 3.6 Quasi-electromechanical oscillation modes before and after auxiliary damping control integration in VSG-SG dual-machine grid-connected system

Quasi-electromechanical Oscillation Mode	Before Auxiliary Damping Control Integration			After Auxiliary Damping Control Integration		
	Eigenvalue	Oscillation Frequency (Hz)	Damping Ratio	Eigenvalue	Oscillation Frequency (Hz)	Damping Ratio
Condition I	0.00169 ± j6.11	0.9724	-32.5	-0.354 ± j6.86	1.0934	0.0516
Condition II	0.0142 ± j6.17	0.9835	-0.023	-0.163 ± j6.19	0.9851	0.0263

Condition III	0.0799 ± j5.94	0.9453	-0.0131	-0.136 ± j6.4	1.0185	0.0212
Condition IV	0.0116 ± j6.09	0.9692	-0.0191	-0.285 ± j6.29	0.9851	0.0379

Table 3.7 Auxiliary damping control parameters under different operating conditions of VSG-SG dual-machine grid-connected system

Auxiliary Damping Control Parameter	Condition I	Condition II	Condition III	Condition IV
K2	107	132	76	217
T1	0.593	0.607	0.539	0.59
T2	0.02	0.016	0.089	0.09
T3	0.593	0.607	0.539	0.59
T4	0.02	0.016	0.089	0.09

Based on the root locus evolution in Figure 13, it is clearly evident that for the quasi-electromechanical oscillation modes under the four operating conditions set in Table 3.6, before and after adding auxiliary damping control to the system, the eigenvalues of the dominant mode shift significantly to the left, with the pole positions moving from λ2,3 to λ'2,3. The leftward shift of pole positions reflects that the introduction of auxiliary damping control substantially increases the damping of the system's quasi-electromechanical oscillation modes, indicating that auxiliary damping control improves system stability to a certain extent. For Condition I, under the operating condition where SG prime mover output and VSG penetration rate both approach critical values, the integration of auxiliary damping control can significantly improve the damping of this quasi-electromechanical oscillation mode. For Condition II, Condition III, and Condition IV, even if SG prime mover output exceeds the critical value, VSG penetration rate is high, or VSG filter impedance is large causing the system to generate quasi-electromechanical oscillations, the introduction of auxiliary damping control also effectively improves the damping of the quasi-electromechanical oscillation modes and enhances system stability.

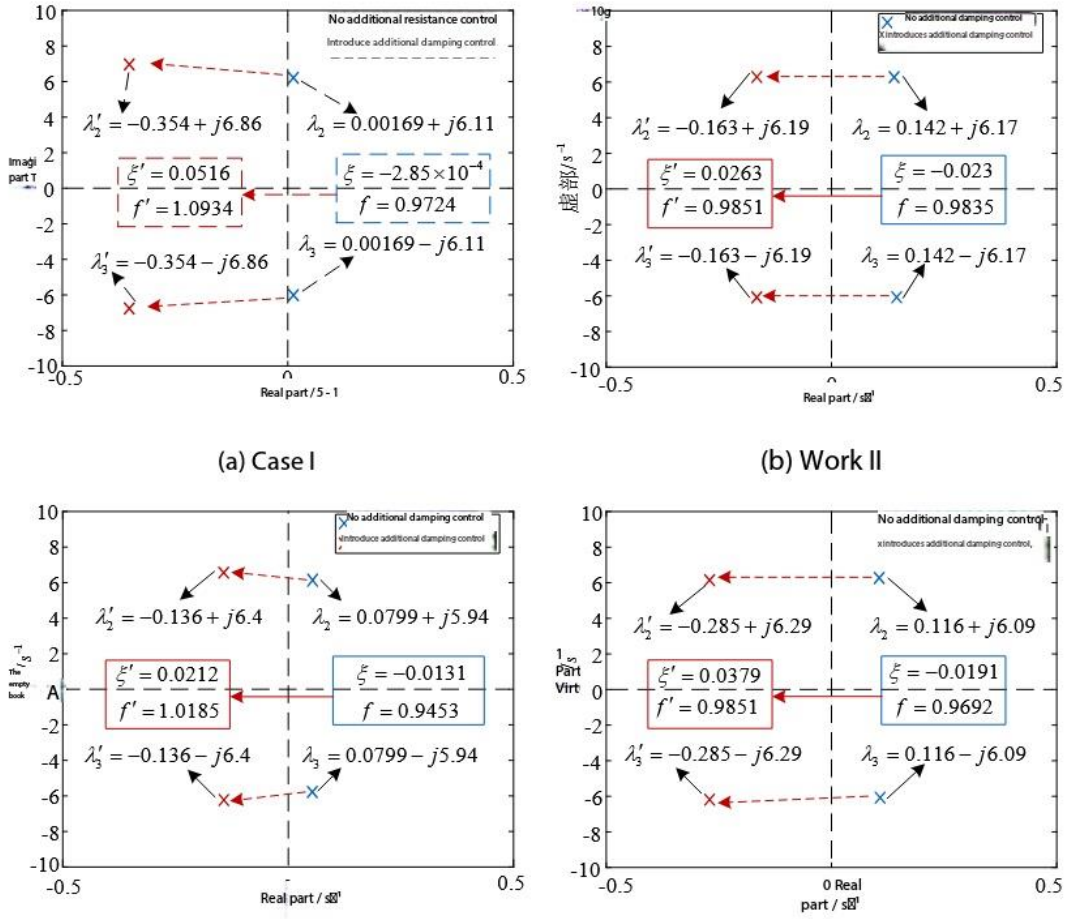

Figure 13 Change trajectory of quasi-electromechanical oscillation modes before and after auxiliary damping control integration of dual machine grid-connected system of VSG-SG

A VSG-SG dual-machine grid-connected system simulation model as shown in Figure 6 was built in MATLAB/Simulink. The four operating conditions were set according to the system parameters in Table 3.5, with other partial parameters as shown in Table 2.2. A three-phase short circuit was set at node g at t=1s. Based on whether the auxiliary damping control is integrated into the VSG-SG dual-machine grid-connected system, the quasi-electromechanical oscillations of VSG output power, VSG virtual power angle, SG output electromagnetic power, and SG physical power angle before and after auxiliary damping control integration under the four conditions are shown in Figures 14-17.

According to the dynamic simulation response characteristics shown in Figure 14, when the system is in the operating condition where SG prime mover output and VSG penetration rate both approach critical values, the system exhibits static stable equilibrium characteristics before disturbance. VSG

output power, VSG virtual power angle, SG output electromagnetic power, and SG physical power angle all maintain static stability. After a three-phase short-circuit fault occurs in the system, the power angle-power dynamic evolution of VSG and SG presents a critical constant-amplitude oscillation mode with an oscillation frequency of about 0.97 Hz and a damping ratio of about -0.00028. Based on the simulation results of quasi-electromechanical oscillations in the VSG-SG dual-machine grid-connected system, the dynamic interaction between VSG and SG units is reflected in both the virtual power angle and physical power angle, as well as the output power of SG and VSG. Additionally, due to the power electronics characteristics of the VSG itself, the VSG output power and virtual power angle generate higher-frequency oscillations at the initial stage of disturbance. These oscillations are caused by the oscillation mode λ6,7 with higher damping characteristics, so they disappear quickly after the disturbance. After introducing the auxiliary damping control strategy, the system's dynamic characteristics change significantly. The power angle-power oscillation frequency of VSG and SG is fine-tuned to 1.10 Hz (relative frequency shift rate 13.4%), and the damping ratio increases to 0.051, forming a typical decaying oscillation mode. This indicates that auxiliary damping control effectively suppresses the quasi-electromechanical oscillations caused by virtual-physical power angle dynamic interaction, which has positive significance for improving the stability of the VSG-SG dual-machine grid-connected system.

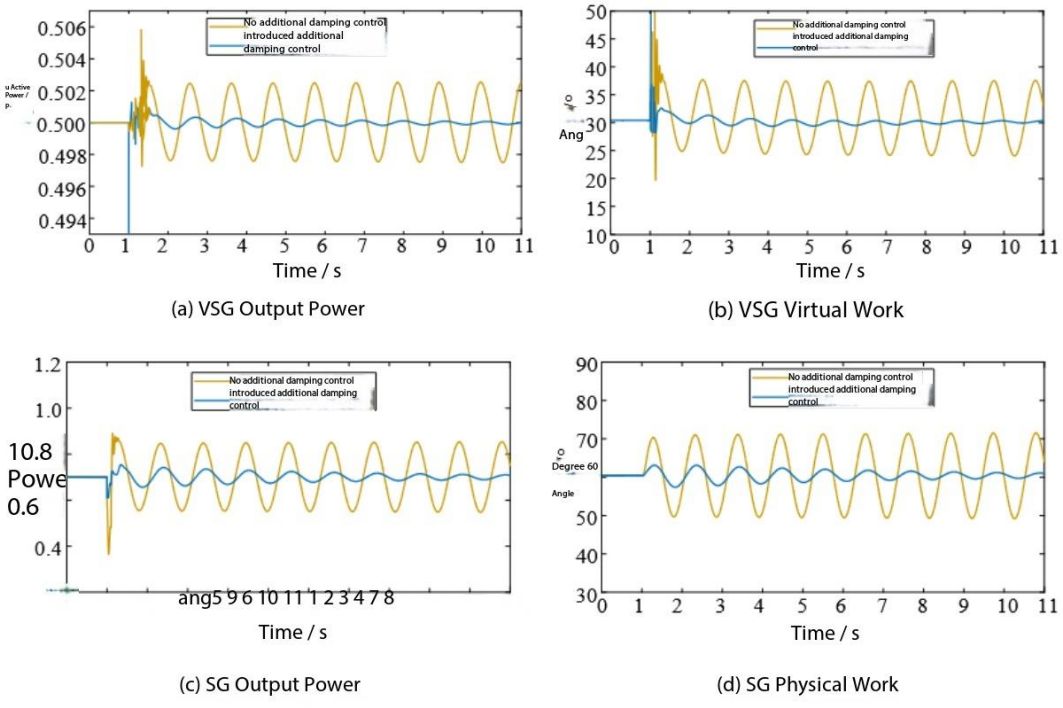

Figure 14 Situation of quasi-electromechanical oscillation modes before and after auxiliary damping control integration at working condition I of VSG-SG dual-machine grid-connected system

When the system is in the operating state of Condition II where SG prime mover output exceeds the critical value and VSG penetration rate is low, according to the simulation results in Figure 15, VSG output power, VSG virtual power angle, SG output electromagnetic power, and SG physical power angle can all maintain static stability before the system is disturbed. After a three-phase short circuit occurs in the system, the power-power angle dynamic oscillation characteristics of VSG and SG deteriorate significantly, showing a negative damping increasing-amplitude oscillation mode with an oscillation frequency of 0.98 Hz and a damping ratio of about -0.02. Compared to Condition I, the rightward shift of the real part of the system eigenvalues under this condition causes the power angle trajectory to exhibit an exponential divergence trend, seriously endangering the stable operation of the system. After introducing auxiliary damping control, the distribution of system eigenvalues is optimized. The oscillation frequency is slightly adjusted to 0.985 Hz (relative frequency shift rate only 0.51%), while the damping ratio increases significantly to 0.0263, achieving a transition from a negative damping state to a positive damping state. Therefore, the introduction of auxiliary damping control significantly enhances the damping characteristics of the system while almost not changing the system oscillation frequency.

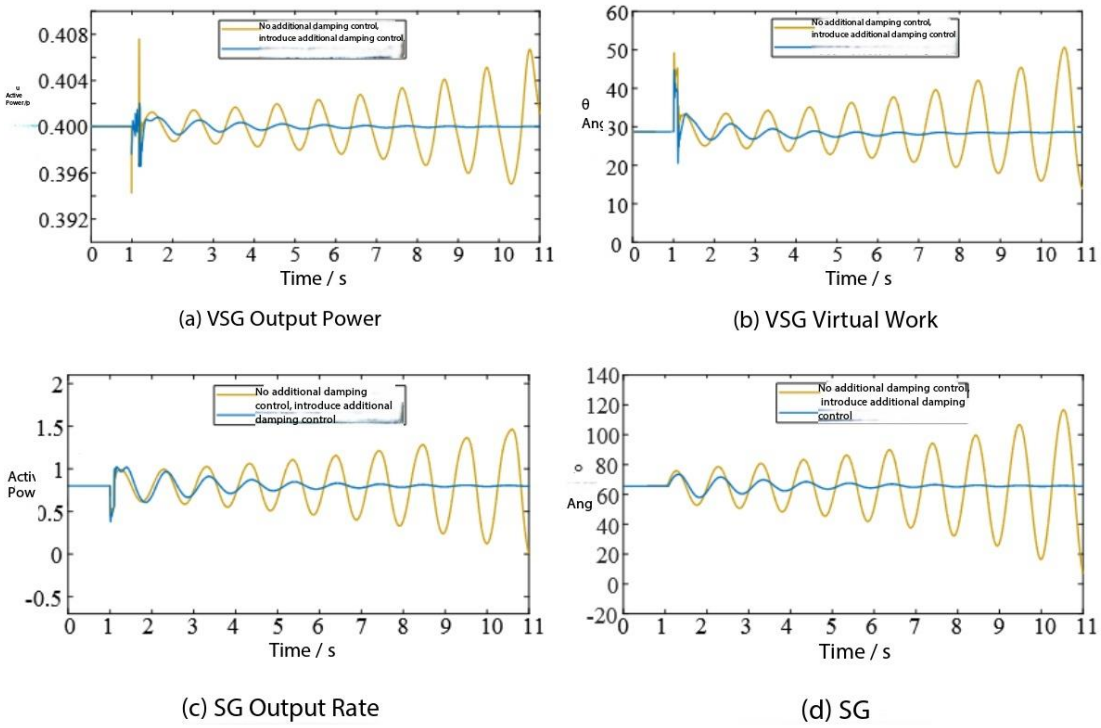

Figure 15 Situation of quasi-electromechanical oscillation modes before and after auxiliary damping control integration at working condition II of VSG-SG dual-machine grid-connected system

For the system in the operating state of Condition III where SG prime mover output is low and VSG penetration rate is high, according to the simulation results in Figure 16, after a three-phase short circuit occurs in the system, the VSG output power and virtual power angle, as well as the SG output power and physical power angle, all exhibit negative damping increasing-amplitude oscillations with an oscillation frequency of about 0.94 Hz and a damping ratio of about -0.013. After auxiliary damping control is introduced into the system, the output power and power angles of the VSG-SG dual-machine grid-connected system then exhibit decaying oscillations with an oscillation frequency of about 1.018 Hz (relative frequency shift rate 8.3%) and a damping ratio of about 0.021, achieving a damping ratio increase of 161.5%. Analysis shows that when VSG penetration rate is high, the introduction of auxiliary damping control significantly enhances the damping characteristics of the VSG-SG dual-machine grid-connected system, effectively suppressing the system's quasi-electromechanical oscillations.

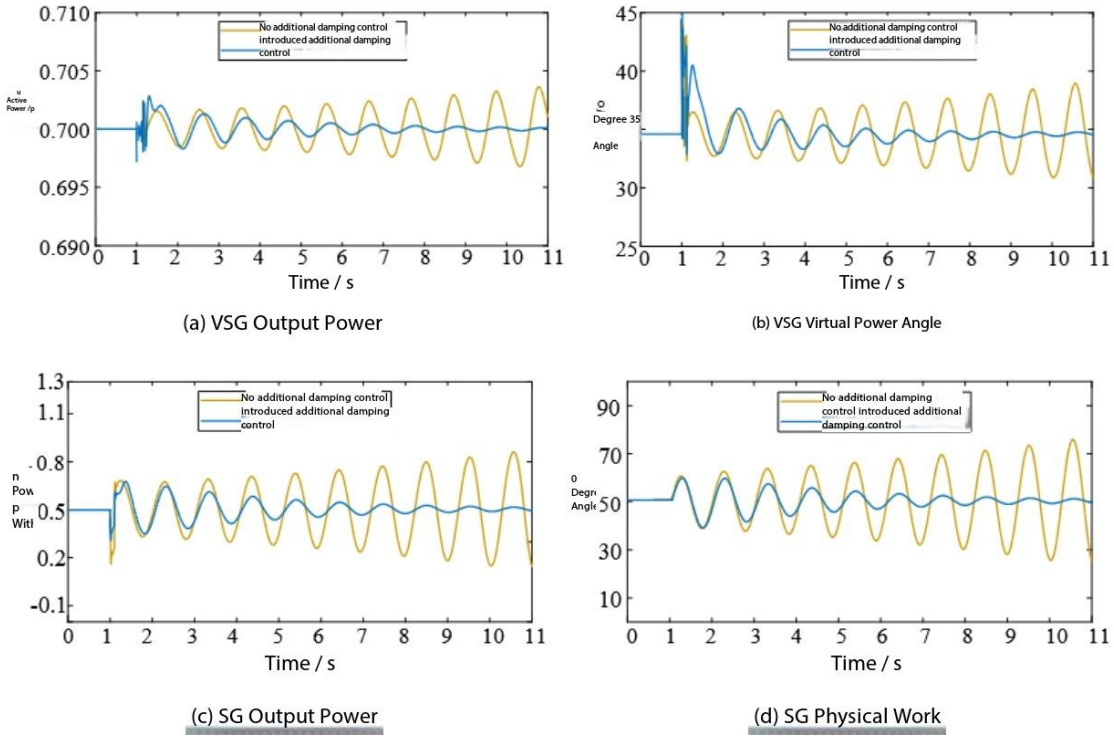

Figure 16 Situation of quasi-electromechanical oscillation modes before and after auxiliary damping control integration at working condition III of VSG-SG dual-machine grid-connected system

From the simulation results in Figure 17, it can be seen that when the system is in the operating state of Condition IV where the VSG filter impedance value is large, after a system fault occurs, the VSG output power and virtual power angle, as well as the SG output power and physical power angle, all exhibit negative damping increasing-amplitude oscillations similar to Condition III, with an oscillation frequency of about 0.97 Hz and a damping ratio of about -0.019. The high filter impedance condition increases the system's equivalent electrical distance, leading to enhanced inertia in the dynamic response of the VSG virtual power angle, which further aggravates the system's quasi-electromechanical oscillations. After auxiliary damping control is introduced into the system, the oscillation frequency is slightly adjusted to 0.98 Hz (relative frequency shift rate 1.03%), and the damping ratio increases significantly to 0.038. Compared to Condition III, the equivalent damping provided by the auxiliary damping control to the system at this time is higher. Analysis shows that when the VSG filter impedance value is large, the system's damping performance with auxiliary damping control is also stronger.

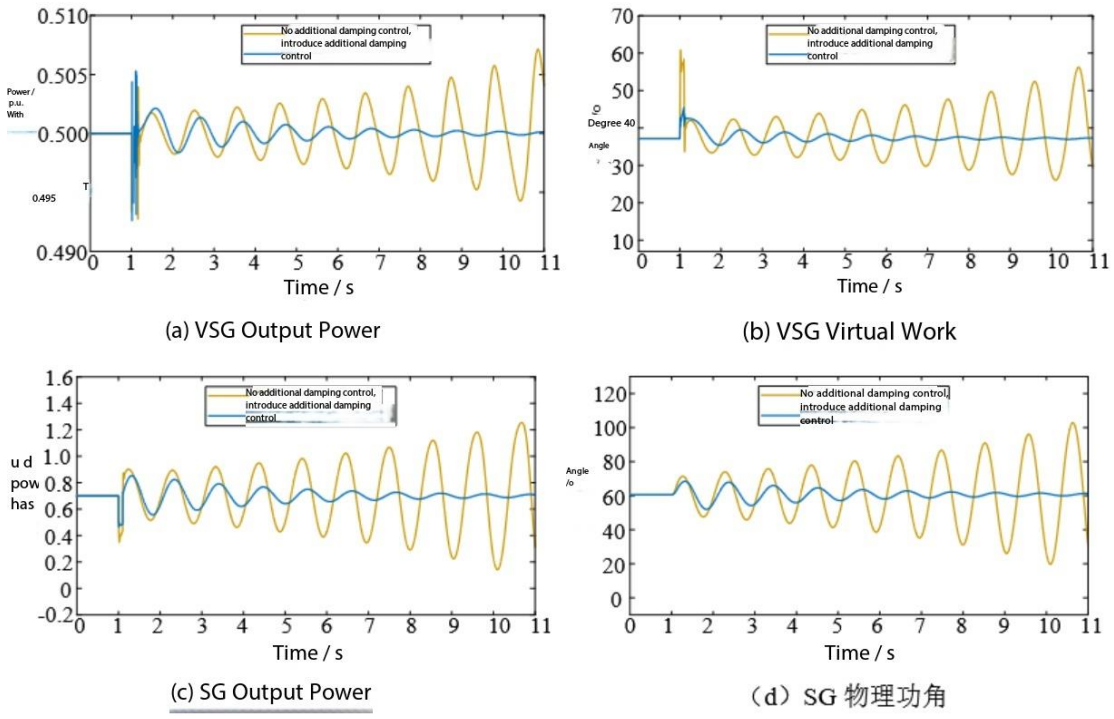

Figure 17 Situation of quasi-electromechanical oscillation modes before and after auxiliary damping control integration at working condition IV of VSG-SG dual-machine grid-connected system

In summary, under different operating conditions including SG prime mover output and VSG penetration rate both approaching critical values, SG prime mover output exceeding the critical value with low VSG penetration rate, SG prime mover output being low with high VSG penetration rate, and large VSG filter impedance value, the system oscillation characteristics vary. Through simulation verification and comparison, it is found that the introduction of auxiliary damping control can effectively improve the system damping characteristics in all cases, achieving effective suppression of quasi-electromechanical oscillations in the VSG-SG dual-machine grid-connected system.

4. Conclusion

This chapter constructed Phillips-Heffron models for both single-VSG and VSG-SG dual-machine grid-connected systems incorporating additional damping control. Using Damping Torque Analysis (DTA), the pathways of the SG-like electromechanical oscillation with the additional damping control were examined. The analytical results demonstrate that the VSG virtual excitation regulator, when accounting for the additional damping control, provides positive damping torque to the VSG's

SG-like electromechanical oscillation loop. This action effectively blocks these oscillations in VSG-based power systems and enhances system stability.

Simulation models for both single-VSG and VSG-SG dual-machine grid-connected systems with the additional damping control were built in MATLAB/Simulink. The simulation results show that the proposed additional damping control strategy shifts the dominant SG-like electromechanical oscillation mode to the left, thereby increasing the system's damping characteristics. Furthermore, by examining different operating conditions and observing the rotor angle and active power oscillations, the results confirm that the additional damping control can effectively suppress SG-like electromechanical oscillations in VSG-based power systems.

Reference

[1] Sun Huadong, Yu Lin, Zhao Bing. Quantitative Analysis Method for Voltage Support Strength of New Energy Grid-connected Systems Based on Steady-state Voltage Safety Constraints after Faults [J] Proceedings of the CSEE, 2023,43 (9) : 3322-3332.

[2] Luo Kui, Guo Jianbo, Wang Weisheng, et al. Analysis and Review of the Impact of Additional Frequency Control for Grid-Following New Energy on Frequency Stability and Small Disturbance Synchronous Stability [J] Proceedings of the CSEE, 2023,43 (4) : 1262-1281.

[3] Liu Zhaoxun, Qin Liang, Yang Shiqi, et al. Review of Virtual Synchronous Control Methods for Power Electronic Converters Oriented to New Power Systems [J] Power Grid Technology, 2023,47 (1) : 1-16.

[4] Sun Huadong, Xu Shiyun, Xu Tao, et al. Analysis on the Definition and Classification of Safety and Stability of Power Systems [J]. Proceedings of the CSEE, 2022, 42 (21) : 7796-7809.

[5] Sun Huadong, Zhao Bing, Xu Shiyun, et al. Definition, Classification and Analysis Method of high-proportion power electronic power system strength [J]. Proceedings of the CSEE, 24, 44 (18) : 7039-7049.

[6] Sun Huadong, Xu Shiyun, He Jingbo, et al. Overvoltage in High Proportion Power Electronics Power System (Part One) : Definition, Classification and Related Requirements [J]. Proceedings of the CSEE, 24, 44 (1) : 22-33.

[7] XIAO H, DUAN X Z, ZHANG Y, et al. Analytically assessing the effect of strength on

temporary overvoltage in hybrid multi-infeed HVDC systems[J]. IEEE Transactions on Power Electronics, 2022, 37 (3): 2480-2484.

[8] Sun Huadong, Yu Lin, Zhao Bing. Quantitative Analysis Method for Voltage Support Strength of New Energy Grid-connected System Based on Transient Overvoltage Constraint [J] Proceedings of the CSEE, 2023,43 (11) : 4207-4218.

[9] Ma Ningning, Xie Xiaorong, He Jingbo, et al. A Review of Wideband Oscillation Research on Power Systems with High Proportion of New Energy and Power Electronic Equipment [J] Proceedings of the CSEE, 2020,40 (15) : 4720-4731.

[10] Chen Lujie, Xu Shiyun, Sun Huadong, et al. Review on Wideband Oscillation of High-Proportion Power Electronics Power System [J]. Proceedings of the CSEE, 2021,41 (07) : 2297-2309.

[11] Zeng Hui, Sun Feng, Li Tie, et al. Analysis of the "September 28" Major Power Outage in Australia and Its Implications for China [J] Automation of Electric Power Systems, 2017,41 (13) : 1-6.

[12] Sun Huadong, Xu Tao, Guo Qiang, et al. Analysis of the "8 • 9" Power Outage in the UK and Its Implications for China's Power Grid [J]. Proceedings of the CSEE, 2019,39 (21) : 6183-6191.